Superscripts

$(\overline{\ })$	= value averaged over volume
$(\ )',(\ )''$	= first, second derivative

Subscripts

c	= active center distribution
o	= optimum distribution
s	= active surface distribution
u	= uniform distribution

LITERATURE CITED

Aris, R., "On Shape Factors for Irregular Particles," *Chem. Eng. Sci.*, **6**, 262 (1957).

Becker, E. R., and J. Wei, "Nonuniform Distribution of Catalysts on Supports: II. First Order Reactions with Poisoning," *J. Catal.*, **46**, 372 (1977).

Butt, J. B., "Catalyst Deactivation," *Chemical Reaction Engineering*, K. B. Bischoff, ed., Adv. Chem. Ser. 109, Amer. Chem. Soc., Washington, DC (1972).

Magee, J. S., "Zeolite Cracking Catalysts—an Overview," *Molecular Sieves—II*, J. R. Katzer, ed., ACS Symp. Ser. 40, Amer. Chem. Soc., Washington, DC (1977).

Ruckenstein, E., "The Effectiveness of Diluted Porous Catalysts," *AIChE J.*, **16**, 151 (1970).

Thomas, C. L., and D. S. Barmby, "The Chemistry of Catalytic Cracking with Molecular Sieve Catalysts," *J. Catal.* **12**, 341 (1968).

Varghese, P., and E. E. Wolf, "Effectiveness and Deactivation of a Diluted Catalyst Pellet," *AIChE J.*, **26**, 55 (1980).

Venuto, P. B., and E. T. Habib, Jr., *Fluid Catalytic Cracking with Zeolite Catalysts*, Marcel Dekker, Inc., New York (1979).

Weisz, P. B., "Zeolites—New Horizons in Catalysis," *Chem. Technol.*, 498 (1973).

Manuscript received May 18, 1981; revision received August 31, and accepted September 16, 1981.

Factors Affecting Secondary Nucleation Rate of Sodium Chloride in an Evaporative Crystallizer

Crystallization kinetics of sodium chloride have been studied in a Continuous Mixed Suspension Mixed Product Removal evaporative crystallizer at 50°C. A marine propeller was found to give a substantially lower nucleation rate than a pitched blade impeller under identical conditions. The crystal turnover time did not affect the effective nucleation rate.

P. A. M. GROOTSCHOLTEN, B. G. M. DE LEER, and E. J. DE JONG

Laboratory for Process Equipment
Department of Mechanical Engineering
Delft University of Technology
Delft, The Netherlands

C. J. ASSELBERGS

Tebodin Consulting Engineers
The Hague, The Netherlands

SCOPE

It has been well established, that one of the main factors, which determine the crystal size distribution (CSD) in an industrial crystallizer is the crystallization kinetics. Controlling the CSD of the product from a crystallizer often implies control over nucleation and growth rate.

From the numerous studies, reported in literature over the past decade, it can generally be concluded that secondary nucleation is the major source of nuclei in industrial crystallizers.

Many authors have studied the phenomenon of secondary nucleation and used their observations to model nucleation kinetics as a function of the operating conditions in an attempt to derive scale-up rules for industrial applications. In spite of these studies, little is known about the mechanism by which secondary nuclei are produced in an industrial crystallizer. So far, this lack of knowledge has hampered attempts to scale up the secondary nucleation process with satisfactory confidence.

The primary objective of this work is to study chemical engineering factors, which affect the performance and scale-up of crystallizer equipment. The experimental work, reported in this paper, is devoted to obtaining the relation between operating conditions, impeller design and crystallizer scale and the salt nucleation rate in an evaporative crystallizer. This study is, moreover, aimed at getting better insight into the intrinsic mechanism of nucleation in order to derive those data, which may have significance for scale-up purposes.

CONCLUSIONS AND SIGNIFICANCE

Experiments have been performed in a 55-L CMSMPR evaporative crystallizer with draft tube-impeller agitation at 50°C. Two types of impeller were employed to study the effect of impeller design on the kinetics of salt nucleation. The process conditions and the type of impeller were found to significantly affect the rate of nucleation. A marine propeller gave rise to a substantially lower nucleation rate and coarser product than a pitched blade impeller under identical operating conditions. From these experiments, it is concluded that the mode of salt nucleation is secondary in nature and that nucleation can primarily be attributed to crystal-impeller collisions. The effect of impeller design on the nucleation rates may be adequately represented by the power numbers of the used impellers.

In order to study the effect of crystal turnover time (circulation frequency) on the rate of nucleation the crystallizer volume was extended from 55- to 91-L effective volume by extending the length of the draft tube and raising the liquor level. To ensure similar impeller-draft tube configuration at 91-L volume, the same marine propeller was used in the 55-L crystallizer. From the experiments performed on both scales, it was found that the turnover time does not affect the effective nucleation rate. It is, therefore, concluded that the turnover time is not an important factor in the scale-up of the nucleation process.

In the studied salt system, abrasion and secondary nucleation occur simultaneously. Abrasion of the largest crystals causes curvature downwards of the experimental CSD, the effect being dependent on operating conditions, impeller-design and, contrary to the nucleation process, the turnover time.

Collision frequencies have been measured independently in an agitated vessel. The results indicate that the collision frequencies strongly increase with increasing particle size. Further, the effect of impeller-speed on collision frequencies is very pronounced. Although these results have only qualitative value, they might have significance for modeling purposes.

MECHANISM OF SECONDARY NUCLEATION

In solutions in which crystals are already present, secondary nucleation is by far the most significant source of nuclei. The supersaturation at which secondary nucleation arises is much lower than that which gives rise to primary nucleation. Having regard to the presence of other crystals, as well as the ensuing relatively low supersaturation, it may be concluded that the nucleation in industrial crystallizers is mainly secondary in character.

The presupposition for the occurrence of secondary nucleation is the presence of other crystals. It is, therefore, natural to suppose that we are concerned with the "breaking loose" of elements in the neighbourhood of crystal surfaces, either as a result of collisions with foreign rigid surfaces (such as walls, impeller or other crystals), or as a result of hydrodynamic shearing stresses. The nucleation mechanisms, discussed in the literature, may on this basis be subdivided into two groups:

Micro-Attrition Mechanisms. Here it is supposed that projections exist on the crystal surfaces, which break off and grow into crystals. Their chance of survival depends on the dimensions of the nucleus. It is a common characteristic of the various microattrition mechanisms, that the nuclei formed already possess a clear crystalline structure, while no visible damage is caused to the parent crystal surface.

Boundary-Layer Mechanisms. It is postulated that clusters of molecules can be liberated from an absorbed boundary layer around a crystal, which is capable of further growth into crystal nuclei. The survival theory will determine whether a phase transition of the fluid cluster to a solid nucleus arises. The suggested mechanism, depending on the degree of supersaturation, is more or less comparable with primary heterogeneous nucleation.

Micro-Attrition

Of the mechanisms of micro-attrition suggested in literature, collision breeding (contact nucleation) is regarded as the most significant mechanism in an agitated crystallizer. It is supposed that small crystalline particles are broken off a parent crystal by hydrodynamic forces or through collision with a foreign body. Both modes of nuclei removal have been established experimentally by Johnson et al. (1972) and Youngquist et al. (1974).

In agitated systems, impacts may be due to collisions with the impeller, the walls of the vessel and with other crystals in the suspension. The forces produced by fluid shear will primarily depend upon the turbulence intensity in the agitated suspension. It may be expected that the forces, exerted by an impact, will normally be larger than fluid shearing forces.

It is generally found that the rate of secondary nucleation increases with the supersaturation, though the dependence is less pronounced than for primary nucleation. The effect may be explained in different ways:

- The micro-roughness of the parent crystal surface could increase with supersaturation so that more nuclei can be dislodged by impact at higher supersaturation.
- The supersaturation determines the size of the critical nucleus.

On the basis of the Ostwald-Freundlich effect, it appears that the critical nucleus size is inversely proportional to the relative supersaturation. Assuming that the small crystalline fragments broken off the parent crystal surface are in the same size range as the critical nucleus at the prevailing supersaturation, an increase in supersaturation would then increase the chance of survival of a nucleus, no matter how it was formed.

This mechanism is often referred to as the survival theory, proposed by Strickland-Constable, and is supported by experimental evidence in the study by Garabedian and Strickland-Constable (1972). Both explanations are consistent with the results of Youngquist et al. (1974), that the nucleation rate is strongly dependent on supersaturation both at the parent crystal and in the region where nuclei develop (survive).

The notion that secondary nucleation is tied up with a micro-attrition process is evidenced by the effects of hardness of the foreign contacting surface. Several authors (Shah et al., 1973; Randolph and Sikdar, 1974; Evans et al., 1974) studied nucleation rates in agitated systems fitted with stainless steel, aluminium and polyethylene impellers, and impellers covered with a soft rubber coating and teflon. It was shown that in all cases the softer polymeric and elastomeric materials dramatically reduce the formation of nuclei, probably by absorbing part of the impact energy.

The important findings also indicate that secondary nucleation may primarily be attributed to crystal-impeller collisions. This may imply that the nucleation rate in a stirred tank crystallizer is a function of the crystal-impeller impact frequency, which will depend on the crystal circulation frequency and impact probability as the crystal passes the impeller. The impact energy may range from a threshold energy, below which no nuclei are generated (Rousseau et al., 1976; Tay et al., 1975), to a maximum which will be proportional to the impeller tipspeed squared.

The role of crystal size in the nucleation process may be twofold: first, the crystal-impeller impact frequency is a function of crystal size; and second, the impact energy is a function of size (mass of the crystal). Several authors using stirred tank crystallizers have demonstrated the influence of seed crystal size and agitator speed on the nucleation rate.

The analysis of the relation between nuclei production and impact frequency is further complicated by the fact that crystals may exhibit a surface regeneration time (Larson and Bendig, 1976; Johnson et al., 1972). When the time between two successive contacts is smaller than the regeneration time, the second impact will yield less nuclei. Regeneration times are longer at lower supersaturations and have been shown to be in the range 7–18 second, (Larson and Bendig, 1976).

As the turnover time (circulation time of the magma) found in small-scale laboratory crystallizers is generally smaller than the regeneration time, the rate of nucleation could become surface-regeneration limited for conditions of high crystal-impeller impact probability. This situation is, however, difficult to visualize, also because it hardly seems likely that exactly the same corner (or edge) is impacted on two successive crystal-impeller contacts. Moreover, the turnover time in large-scale industrial crystallizers is of the order of 60 s.

The nucleation rate will then definitely be limited by the rate of nuclei removal from the parent crystal surface due to crystal collisions. This was already suggested by Evans et al. (1974) on the basis of experimental results, obtained in a continuous ice crystallizer. On the basis of these observations, it may be expected that regeneration time is not an important factor in the scale-up crystallizer equipment.

Other "Sources and Sinks" of Nuclei

It is of interest to note that abrasion and secondary nucleation may simultaneously occur under conditions of vigorous agitation. Abrasion is exhibited by the presence of large amounts of randomly shaped crystal fragments, which are generally smaller than 50–100 μm, and by rounding off of the sharp corners and edges of the larger crystals. Although the size of crystal fragments and secondary nuclei will be different, abrasion will enhance the rate of nucleation, provided that the fragments grow.

A sink of nuclei may be the selective dissolution of the smallest crystals in zones of undersaturation. In a large-scale evaporative salt crystallizer, undersaturation may be produced in the calandria due to heating-up of the circulating slurry. In a theoretical analysis of fines dissolution in the circulation loop of an external forced-circulation salt crystallizer (Asselbergs and de Jong, 1972), it was shown that the size of the crystals which do not survive is in the order of 3–5 μm (dissolution time: 4–5 s, magma temperature rise: 2–5°C). Obviously, undersaturation may partially offset secondary nucleation and the production of abrasion fragments.

THEORETICAL AND EMPIRICAL MODELS

Experimental observations presently available permit the belief that secondary nucleation involves a micro-attrition mechanism and results from crystal-impeller, crystal-wall and crystal-crystal collisions. It is usually accepted that the major contribution to the overall nucleation rate is in the crystal-impeller collisions. In Figure 1, an attempt has been made to demonstrate the complex interrelation between the factors affecting the rate of secondary nucleation due to crystal-impeller collisions. Although this diagram is by no means complete, it may serve the purpose of illustrating that the development of theoretical nucleation models is exceedingly complex.

Considering the complexity of the phenomenon of secondary nucleation, the various models presented in the literature are by necessity based on oversimplified assumptions. The available nucleation expressions are of restricted, practical use and cannot yet be used for *a priori* evaluation of the nucleation rate. Nevertheless, theoretical models may support the assessment of probable interaction of process configuration and operating conditions with system kinetics.

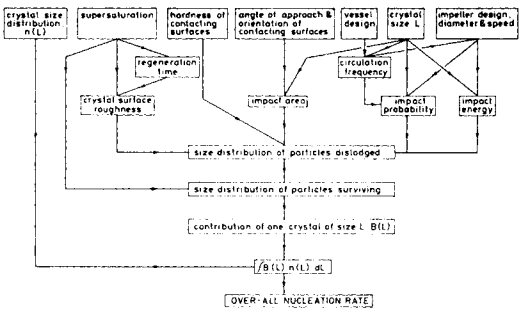

Figure 1. Interrelation scheme.

As long as the understanding of the intrinsic mechanism of secondary nucleation remains incomplete, experimental data may be correlated by an empirical power law relation of the form:

$$B^0 = k.(\Delta C)^p.\mu_i^s \qquad (1)$$

where μ_i is one of the moments of the CSD accounting for the presence of crystals. By qualitative reasoning, it has been assumed that secondary nucleation is dependent on either the number of crystals, crystal perimeter, area or mass. These factors might be taken into account through 0th, 1st, 2nd or 3rd moment respectively of the population density distribution. The constant k in Eq. 1 is a parameter, which may be a function of the vessel geometry, dimensions of the impeller, impeller-design and speed, as well as of temperature and of the physical and chemical properties of the materials.

Since the supersaturation in high-yield systems is generally immeasurably low, ΔC in Eq. 1 may be conveniently replaced by growth rate.

In the present work, the results will be correlated by a generalized power law relation as has been used on many previous occasions:

$$B^0 = k_B.N^h.G^i.M^j \qquad (\#/m^3{\cdot}s) \qquad (2)$$

where N is the impeller speed (1/s), k_B is the nucleation rate coefficient and h, i, and j are empirical sensitivity parameters.

EXPERIMENTAL

Basis of Design

As outlined previously, the work conducted in the semitech crystallizer with internal calandria and internal circulation was primarily aimed at eliciting nucleation kinetics for sodium chloride as function of crystallizer design, scale and operating conditions. To attain this object, the MSMPR concept can be fruitfully used. The experimental system was, therefore, designed so that conditions of mixed suspension and mixed product removal were as nearly as possible achieved.

In order to produce a well-mixed crystal suspension with uniform properties, special attention was paid to the hydraulic design of the vessel. It was decided to use a vessel with draft tube agitation to create a well-defined flow pattern. Moreover, to ensure off-bottom suspension and to eliminate dead zones underneath the impeller, a special profiled bottom was utilized. The cross-sectional area of the cylindrical draft tube was equal to the area of the vessel draft tube annulus (equal velocity configuration). A relatively large impeller, running at reasonable speeds, was chosen to give sufficiently high liquid velocities to circulate the crystals with the liquid. The hollow draft tube also served as a double-pipe heat exchanger.

Representative and continuous product removal was achieved via a discharge pipe mounted parallel to the main flow path in the vessel draft tube annulus. A series of interchangeable off-take tubes of different diameter was available to meet isokinetic conditions under all relevant circumstances.

Description of 55-L Crystallizer

The experimental unit which was developed on the basis of the above principles is shown in Figure 2.

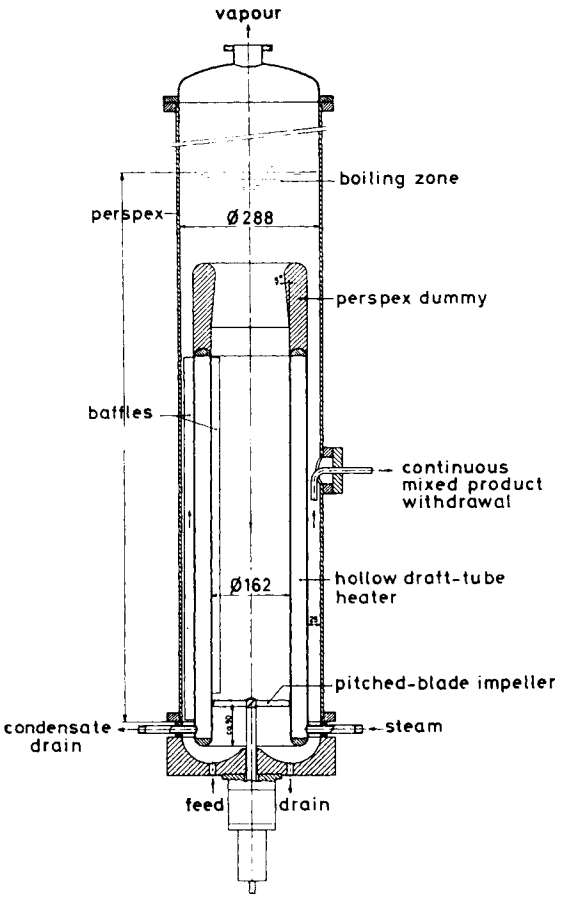

Figure 2. 55 ltr. Crystallizer with internal circulation.

The cylindrical evaporator body had an inside diameter of 288 mm and was made of plexiglass to allow visual observation of the circulating suspension. The profiled plexiglass bottom was shaped in such a manner that the cross-sectional area perpendicular to the contours of the hemispherical bottom end of the draft tube remained constant. The clearance of the draft tube from the base was 33 mm. All crystallization experiments were carried out at approximately 50°C. A bottom-entering impeller acted as an axial flow pump within the draft tube located centrally in the vessel. The inside diameter of the draft tube was 162 mm, which is equal to the pump-chamber diameter of the circulation pump used in the pilot plant as described by Grootscholten et al. (1980).

Two types of impellers were used to study the effect of impeller design on the nucleation rate: a stainless-steel pitched-blade impeller (four blades at 45°, diameter = 157 mm) and a stainless-steel three-bladed pitch one marine-type propeller (diameter = 155 mm). The draft tube was provided with eight vertical baffles to eliminate vortexing (four on the inside, 16 mm in width; four on the outside, 19 mm in width). The flow pattern was down the draft tube. To minimize heat short-circuiting, the top end of the draft tube was additionally fitted with a specially shaped plexiglass "dummy."

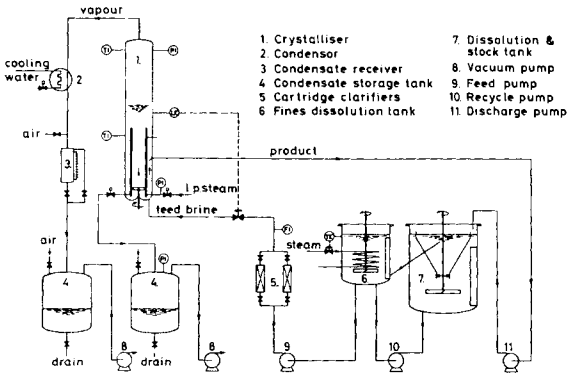

Figure 3. Process flow diagram of experimental facility.

The length of the dummy was 195 mm and the minimum inside diameter at the pear-shaped top was 142 mm. This arrangement also prevented flashing of the liquid due to a pressure drop over the entry of the draft tube. This liquid level was about 0.2 m above the top of the dummy.

The length of the draft tube was changeable, which enabled the crystallizer volume to be extended from 55 to 91 L effective volume. Product removal was continuously effected through an elbow outlet pipe, which was placed in the annulus. The inside diameter of the interchangeable elbows was in the range 5–10 mm. The feed brine was introduced into the base of the evaporator. Vapors left the vessel through the top outlet and were condensed in a coiled glass tube condenser. A schematic diagram of draft tube crystallizer and associated equipment is depicted in Figure 3.

Hydraulic Characteristics of Internal Loop System

Considering the effects of hydrodynamics on crystallization kinetics, it is of interest to establish the hydraulic characteristics of the system. Important parameters are the impeller pump constant k_p (from $\phi_v = k_p N d^3$) and the impeller power number P_o (from $P = P_o \rho N^3 d^5$). The former has been evaluated from measurements of the prevailing fluid velocities at various impeller speeds. Such measurements are also necessary in order to achieve isokinetic product removal and to establish the turnover time. From the flow measurements, it was found that the axial velocity is a linear function of the impeller speed and that the pumping capacities of both impellers are the same. For both impellers, the pump constant k_p was found to be 0.5.

The power number can be obtained from measurements of the power consumption of the system as a function of the impeller speed. The power consumed by the agitator was determined from measurements of the electric power admitted to the electromotor. A watt-meter was employed to measure the total power consumption, which included the friction losses in bearings and seals and the losses in the electromotor. These losses were compensated for by also performing the measurements with the empty system. Since the losses account for a substantial part of the total power consumption, the technique employed is not very accurate. The experiments were conducted with water at ambient temperature. For the pitched-blade impeller, a value of 0.32 was established, whereas the propeller was more efficient, having a power number of 0.13.

Operating Conditions

To investigate the effect of operating conditions on the rate of nucleation, these variables should be varied over as large a range as possible within the technically feasible limits. The variables investigated are: impeller speed, residence time, and vapor production rate.

The range of these variations, in so far as this can be regarded as relevant for secondary nucleation, are:

Variable	Minimum	Maximum
Impeller Speed	7	13 cps
Vapor Production Rate	2.5×10^{-3}	10×10^{-3} kg/s
Residence Time	0.3	0.9 hour

The residence time is only varied by way of the volumetric production rate. Initially the operating volume was 55 L. The vapor temperature was approximately 55°C in all experiments. For all experimental work, technical salt and demineralization water were used.

Sampling, Sample Treatment and Sieve Analysis

The crystallizer was normally operated for at least ten residence times to achieve steady state. At the end of each experimental run, two samples of approximately 80 g (dry salt) each were taken from the isokinetic product removal stream. Before sampling, a small amount of inhibitor (0.5 g ferro-cyanide) was added to the sample flask to minimize changes in the CSD resulting from crystal growth or dissolution during sampling and sample treatment. The carrier brine was removed from the samples by filtering. Then the samples were washed with an ethanol-water mixture to remove residual brine. Finally, the samples were washed with pure ethanol and two times with pure di-ethylether. The salt crystals were dried under an infrared lamp.

The crystal size distribution was measured using VECO precision sieves, featuring a flat nickel screen with square holes. Apertures of the 17 sieves employed were based on a 74-μm screen and increased by a factor $2^1/_4$ from 44 to 837 μm (approximating the Americal Tyler scale).

Sieve analysis was carried out using a Derritron (type VP 85) shaking machine (frequency: 50 cps; acceleration: 4 g; vertical amplitude: 0,4 mm; sample weight: 80 g; sieving time: 60 min). Attrition of the crystals during sieving was found to be negligible under these conditions.

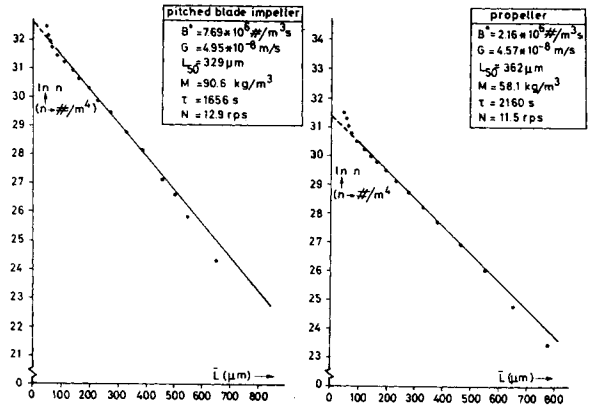

Figure 4. CSD's for the 55 litre crystallizer obtained with the pitched blade impeller and marine propeller.

Population density distributions have been calculated from the sieve analysis data. Values of $k_v = 1$ and $\rho_s = 2{,}155$ were consistently used in the evaluation of the population densities. Mean crystal sizes were determined on the basis of the cumulative weight distributions.

RESULTS

Growth and Nucleation Rates

On the basis of the population balance theory, B^o and G can be readily derived from the crystal-size distribution of a CMSMPR-system. If McCabe's ΔL law holds, Eq. 3 gives the fundamental relationship between the population density n and crystal size L:

$$n = n^o \exp[-L/G\tau] \tag{3}$$

Plotting the logarithm of population density vs. size gives a straight line with a slope of $-1/G\tau$ and an intercept at $L = o$ of n^o. If the mean residence time is known, the linear growth rate G can thus be calculated. On the basis of the definitions of n^o and G, it can be shown that:

$$B^o = n^o G \tag{4}$$

In the present work, values of the linear growth rate were obtained from the slope of the best straight line through the experimental population density distributions. Effective nucleation rates were calculated from the magma concentration equation for a CMSMPR-system, which reads:

$$M = 6k_v\rho_s n^o(G\tau)^4 = 6k_v\rho_s B^o G^3\tau^4 \tag{5}$$

So that:

$$B^o{}_{\text{eff}} = \frac{M}{6k_v\rho_s G^3\tau^4} \tag{6}$$

Crystallization Experiments 55-L Crystallizer

As mentioned earlier, the rate of nucleation and the rate of growth can be conveniently correlated by an empirical power law relation of the form:

$$B^o = k_B N^h . G^i . M^j \qquad (\#/\text{m}^3\text{·s}) \tag{2}$$

In order to determine the kinetic exponents and the rate coefficient, k_B, experiments were conducted over a wide range of the three independent variables, N, τ and ϕ_{mv}. Two types of impeller were moreover used to study the effect of impeller design on the empirical constants.

Resulting data were in the following ranges:

	Propeller	Pitched-Blade Impeller
L_{50} (μm)	320–422	254–458
G (nm/s)	30–85	30–80
B^o (10^6 #/m^3·s)	1–7	1–8

Figure 4 shows typical steady-state population density distributions obtained with the pitched blade impeller and the marine propeller respectively. It can be seen that the data can be correlated by straight lines over a substantial crystal size range. For sizes below 100 μm, a steep increase in population density is always found, whereas curvature downwards occurs in the larger size range, where rounded crystals are generally found.

To check the quality of the results obtained from the population density distributions, the resulting values of G were used to evaluate

TABLE 1. RESULTS FROM 55-L PITCHED-BLADE IMPELLER

Run	M (kg/m^3)	τ (s)	N (rps)	G (10^{-8} m/s)	n^o (10^{13} #/m^4)	B^o (10^6 #/m^3·s)	L_{50} (μm)
B 1.	77.8	1286	8.55	7.44	7.17	5.33	390
B 2.	54.6	1006	11.25	8.12	9.38	7.62	404
B 3.	64.6	1285	8.55	7.46	5.93	4.42	281
B 4.	76.3	1500	8.55	6.74	5.65	3.81	404
B 6.	74.7	1732	7.00	6.05	4.79	2.89	—
B 9.	36.5	1081	6.95	7.93	6.33	5.02	355
B 10.	42.6	1225	9.45	7.09	5.79	4.11	358
B 15.	55.9	1362	6.95	8.01	3.05	2.44	436
B 16.	89.3	1601	9.85	5.94	8.44	5.01	376
B 17.	90.6	1656	12.95	4.95	15.54	7.69	329
B 18.	71.5	3037	6.95	3.66	3.62	1.32	455
B 19.	85.8	3134	9.85	3.14	7.01	2.20	396
B 20.	76.1	2233	6.95	5.45	2.68	1.46	439
B 21.	77.2	2160	9.85	4.30	8.01	3.44	378
B 22.	65.2	2397	12.95	3.45	10.78	3.72	334
B 23.	76.0	1440	10.95	6.40	8.14	5.21	351
B 24.	76.6	1440	8.4	6.78	6.52	4.42	393
B 25.	74.4	2160	7.4	5.29	3.37	1.77	426
B 26.	91.3	2880	7.4	4.04	3.85	1.56	458
B 27.	76.3	2880	10.7	3.09	9.38	2.90	370
G 1	72.1	1800	11.3	4.85	9.60	4.66	324
G 2	70.9	1800	8.4	5.72	4.87	2.79	384
G 3	71.2	1800	6.9	6.51	2.92	1.90	412
G 4	72.1	1800	9.4	5.22	7.14	3.73	397
G 5	71.6	1800	13.0	4.96	8.70	4.32	313
G 6	71.2	1800	6.9	6.54	2.87	1.88	412

TABLE 2. RESULTS FROM MARINE PROPELLER

Run	M (kg/m^3)	τ (s)	N (rps)	G (10^{-8} m/s)	n^o (10^{13} #/m^4)	B^o (10^6 #/m^3·s)	L_{50} (μm)
G 7	73.7	1800	7.3	5.63	5.40	3.04	392
G 8	73.4	1800	8.6	5.52	5.83	3.21	371
G 9	68.0	1800	10.0	5.93	4.04	2.40	387
G 10	68.3	1800	11.6	5.59	5.15	2.88	356
G 11	72.2	1800	13.3	5.27	6.89	3.63	346
G 12	69.8	1800	10.0	5.73	4.76	2.72	393
G 13	70.5	1800	11.6	5.69	4.94	2.81	380
G 14	63.0	1800	7.1	5.76	4.23	2.43	400
G 15	67.1	1800	7.1	6.37	3.00	1.91	422
G 16	64.4	1800	8.7	5.88	3.97	2.33	388
G 17	66.6	1800	10.1	5.79	4.38	2.53	386
G 18	64.9	1800	11.6	5.56	4.98	2.77	368
G 19	60.1	1800	13.4	5.34	5.44	2.91	350
G 20	70.4	1440	11.5	6.72	6.20	4.17	365
G 21	68.6	2160	11.5	4.92	4.15	2.04	393
G 22	76.2	1080	11.6	8.51	8.28	7.04	348
G 23	71.4	2880	11.5	3.93	3.37	1.32	398
G 25	64.8	2160	11.5	4.75	4.52	2.14	368
G 26	79.8	1440	11.6	6.79	6.72	4.56	366
G 27	113.0	2160	11.6	5.08	6.03	3.07	379
G 28	195.0	3240	11.5	3.53	8.73	3.08	404
G 29	110.7	1800	11.5	5.94	6.53	3.88	380
G 30	125.0	2880	11.5	4.06	5.18	2.10	390
G 31	82.9	1800	11.5	5.78	5.44	3.14	377
G 32	31.2	1800	11.5	5.50	2.51	1.38	364
G 33	32.9	2160	11.5	4.12	4.04	1.67	320
G 34	46.7	2160	11.5	4.48	4.13	1.85	354
G 35	58.1	2160	11.5	4.57	4.73	2.16	362
G 36	24.7	1800	11.6	5.64	1.80	1.01	369
G 37	127.2	2880	11.6	3.95	5.90	2.33	398

the mean crystal size on the basis of the well-known CMSMPR-equation, which reads

$$L_{50} = 3.67.G.\tau \qquad (7)$$

The average deviation between theoretical and experimental values of L_{50} is about 4% with a maximum of 12%, which can be attributed to curvature downwards exhibited by the experimental distributions. These results confirm that the developed crystallizer reasonably approximated the ideal CMSMPR-performance. Nucleation rates, growth rates, nuclei population density, mean crystal size and operating conditions are given for pitched blade impeller and propeller in respectively Tables 1 and 2.

From Tables 1 and 2, it can be qualitatively inferred that a coarse product is obtained at low impeller speeds and at high residence times. These conditions give rise to relatively low values of nucleation rate and crystal growth rate. At constant impeller speed both the nucleation rate and the growth rate were found to decrease with increasing residence time. At constant residence time on the other hand, an increase in impeller speed resulted in a higher nucleation rate and hence lower growth rate. Further it may be established that an increase in magma concentration results in an increase in nucleation rate, whereas the crystal growth rate remains constant, provided a constant residence time and impeller speed.

The effect of impeller design on crystallizer performance is best illustrated by the crystal size distributions shown in Figure 5. It can be seen that the effects are not very dramatic. For similar operating conditions the propeller produces a somewhat coarser product as result of a lower nucleation rate and higher growth rate. Moreover curvature downwards of the population density distribution in the largest size range was less for the propeller, which suggests that this design causes less damage to the crystals.

Correlation of Kinetic Data of 55-L Crystallizer

To provide a quantitative basis for the interpretation, the results for the pitched-blade impeller and the propeller have been successfully correlated by a power law relationship as proposed earlier. For the propeller, the resulting correlation is:

$$B^o = 1.0 \times 10^{17} \times N^2G^2M \qquad (\#/m^3\cdot s) \qquad (8)$$

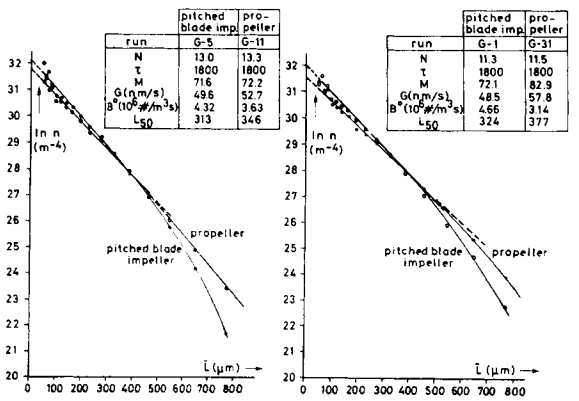

Figure 5. Effect of impeller design on CSD (N = 13 rps). Effect of impeller design on CSD (N = 11 rps).

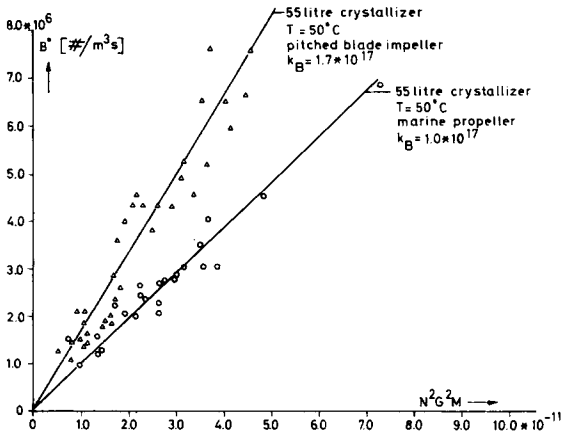

Figure 6. Effect of impeller design on the effective nucleation rate.

TABLE 3. EXPERIMENTAL RESULTS FROM 91-L MARINE PROPELLER

Run	M (kg/m^3)	τ (s)	N (rps)	G (10^{-8} m/s)	n^o (10^{13} #/m^4)	B^o (10^6 #/m^3·s)	L_{50} (μm)
S 1	46.7	2376	10.9	4.57	2.60	1.19	400
S 2	50.7	2022	9.9	5.48	2.60	1.42	430
S 3	53.4	1928	11.1	5.45	3.40	1.85	425
S 4	51.4	2034	12.0	5.10	3.43	1.75	395
S 5	54.3	2131	9.0	5.36	2.47	1.32	440
S 6	51.3	1774	12.9	5.53	4.39	2.43	348
S 7	60.5	2820	7.2	5.04	2.12	1.07	481
S 8	53.8	2258	8.0	5.34	1.97	1.05	470
S 9	61.4	4212	10.9	3.18	1.48	0.47	500
S 10	43.5	2124	9.1	5.41	1.93	1.04	440

The resultant correlation for the pitched blade impeller is:

$$B^o = 1.7 \times 10^{17} \times N^2G^2M \qquad (\#/m^3\cdot s) \qquad (9)$$

Both correlations are graphically represented in Figure 6.

Experimental Work 91-L MSMPR Crystallizer

In order to study the effect of turnover time (circulation frequency) on the rate of nucleation the crystallizer volume has been extended from 55 to 91 L active volume by extending the length of the draft tube from 800 mm up to 1,800 mm. From flow measurements it was established that extension of the volume does not significantly affect the flow characteristics, which implies similar circulation rates for similar impeller speeds. Pressure drop over the internal circulation loop is most likely to be due to the flow inversions at top and bottom end of the draft tube.

Crystallization experiments were carried out in the same range of operating conditions as quoted for the 55-L crystallizer. To ensure similar impeller draft tube configuration at 91-L volume the same marine propeller was used as used in the 55-L crystallizer.

The resulting data were in the following ranges:

L_{50} (μm)	350–500
G (nm/s)	35–60
B^o (10^6 #/m^3·s)	0.5–2.5
n^o (10^{13} #/m^4)	1.5–4.4

A listing of the resultant values of nucleation rate, growth rate, nuclei population density, mean crystal size and operating conditions is given in Table 3. The average deviation between theoretical and experimental mean crystal size is less than 3% with a maximum of 8%. These results indicate that the 91-L crystallizer better approximated the ideal CMSMPR-performance than the 55-L crystallizer. This can be attributed to the fact that the experimental curve obtained from the 91 litre crystallizer exhibits less curvature downwards in the large size range than a distribution obtained from the 55-L crystallizer under similar conditions.

The results have been correlated by a similar power relation as was used to correlate the data obtained from the 55 litre crystallizer. For the 91-L crystallizer equipped with the marine propeller the resulting correlation is:

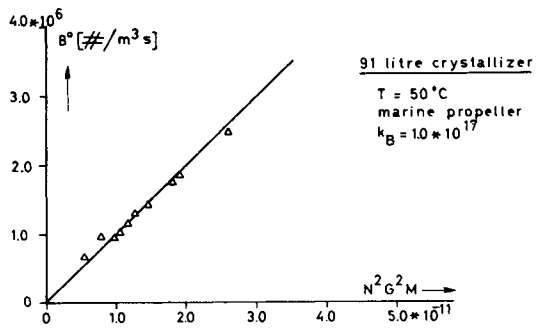

Figure 7. Determination of k_B for marine propeller and 91 litre volume.

$$B^o = 1.0 \times 10^{17} \times N^2G^2M \qquad (\#/m^3\cdot s) \qquad (10)$$

This relation is graphically represented in Figure 7.

DISCUSSION OF KINETIC RESULTS

From the postulated correlations (Eqs. 8, 9 and 10) it can be concluded that the kinetic exponents are not a function of impeller design or crystallizer scale.

At 50°C, the growth rate of sodium chloride crystals is approximately first order in supersaturation (Scrutton and Grootscholten, 1981). Since a value of $i = 2$ was obtained in the present work, the dependence of the nucleation rate on supersaturation will be approximately second order. This low order suggests that the mode of nucleation is secondary rather than primary in nature. The observed value of i is close to the values of 1.76 and 2.4 reported by Koros et al. (1972) and Liu and Botsaris (1973) for the NaCl-ethanol salting out system. Recent analysis of the data presented by Koros et al. (1972), taking into account the effect of impeller Reynolds number on the crystal growth rate, reveals that the nucleation rate in the salting out system is roughly proportional to Re^2, which actually comes to N^2. This is in good agreement with the present experimental findings. The kinetic exponents, found in this study, are similar to those obtained by Scrutton (1979) in a 10-L evaporative CMSMPR-crystallizer at 108°C.

Since in the postulated power law relation the growth rate depends on the nucleation rate via the mass balance and consequently on the impeller design at constant M, τ and N it is more realistic to analyze and compare the effects of impeller design and crystallizer scale on the nucleation rate on the basis of residence time instead of the growth rate. In Relation 2, the growth rate can be replaced by τ by combination of this relation with the CMSMPR-relation for the magma concentration, Eq. 5. Using a volume shape factor $k_v = 1$ and a solids density $\rho_s = 2{,}155$ kg/m^3 it can be demonstrated that the nucleation rate B^o can be written as:

$$\frac{B^o}{M} = 0.023 \times k_B^{0.6} \times N^{1.2} \times \tau^{-1.6} \qquad (11)$$

Using the values found for the rate coefficient, k_B, at 55 L it can be seen that the pitched blade impeller gives a nucleation rate, that is 50% higher than the nucleation rate obtained with the propeller under identical conditions. Since the pumping capacities of both impellers are the same, giving the same velocities and circulation times, it is clear that the difference in nucleation rates may be primarily attributed to the design of the impeller. The overall results indicate that crystal-impeller collisions or interactions play a dominant role in the formation of nuclei. The linear relationship between nucleation rate and magma concentration argues in the same direction.

The difference between the proportionality constants in the nucleation equations for the propeller and the pitched-blade impeller ($k_B = 1{,}0.10^{17}$ respectively $1.7.10^{17}$) is appreciably smaller if the nucleation rates are related to specific power input rather than impeller speed. Using the power numbers reported previously,

the nucleation rate correlations (Eqs. 8 and 9 resp.) can be rewritten in terms of the specific power input ϵ ($\epsilon = P_o N^3 d^5/V$) as follows.

Propeller:

$$B^o = 2.7\ 10^{19}\epsilon^{2/3}G^2M \tag{12}$$

Pitched-Blade impeller:

$$B^o = 2.5\ 10^{19}\epsilon^{2/3}G^2M \tag{13}$$

This observation tentatively suggests that in the 55-L crystallizer the effect of impeller design may be adequately represented by the specific power input, i.e., the impeller power number.

From the experiments conducted in the 55 and 91 L crystallizer, it can be concluded that for identical N, τ and M both scales produce the same effective nucleation rate per unit crystallizer volume. This observation indicates that the crystal turnover time and consequently the circulation frequency of the crystals do not affect the effective nucleation rate. It may therefore be concluded, that the turnover time is not an important factor in the scale-up of the nucleation process. This conclusion is in conformity with the suggestion in a previous paragraph: The nucleation rate in a large scale crystallizer is most likely dominated by the rate of nuclei removal from the parent crystal surface due to crystal-impeller interactions. In this light a surface regeneration time (and consequently the turnover time) was not expected to be an important factor in the scale-up of crystallizer-equipment.

The nuclei removal rate may be expected to be a function of the number of impacts on the impeller and the energies of these impacts, no matter the history of the colliding crystals. The number rate of impacts depends on the number of crystals passing the impeller-region and the probability to collide with the impeller. It is not a matter of speculation to state that number rate of impacts and impact energy are both functions of crystal size, impeller speed and design.

DEVIATIONS FROM STRAIGHT-LINE DISTRIBUTION

Figure 4 shows typical steady-state population density distributions obtained with the pitched-blade impeller and the marine propeller respectively. For sizes below 100 μm, the distribution deviates from the extrapolated straight line by steeply increasing with decreasing size. Curvature downwards occurs in the larger size ranges, where rounded crystals are generally found.

Accumulation of Fines

In the small-size range, there is a relatively high scatter of the points about the experimental curve due to the reduced reliability of the sieve analysis in this region. Moreover, while population densities are systematically calculated on the basis of a volume shape factor $k_v = 1$, microscopic observations of the smallest particles reveal the presence of substantial amounts of randomly shaped crystalline fragments with a shape factor larger than 1. The difference between experimental curve and extrapolated straight line could, however, not be declared on basis of the actual shape factor. Since abrasion fragments are known to exhibit very low growth rates (Van't Land and Wienk, 1976; Bujac, 1976), indeed they are not found in the intermediate size range, the average growth rate in the smallest size ranges may be smaller than the rate of growth of undamaged particles and particles in the range free from breakage effects.

This anomalous growth behavior reduces the slope of the CSD and this gives rise to a steep increase in population density. In the present case, the observed deviation may therefore presumably be attributed to the accumulation of abrasion fragments. As consequence of the deviations in the small size ranges, the real nucleation rate can only be determined on the basis of a detailed study of the CSD in the smallest size ranges. In the present work the rate of nucleation is by necessity approximated by the effective nucleation rate, which may be found from extrapolation of the mainly linear distributions.

Abrasion of Large Crystals

For crystal sizes larger than 500 μm, curvature downwards generally occurs. While cubic habit crystals are normally produced in the size range 100 to 500 μm, the larger crystals are rounded to varying degrees depending on the operating conditions, impeller design and crystallizer scale. The extent of rounding increased with size and particles in the size range 837–996 μm are completely spherical (volume shape factor was found to be of order of 0.5). However, this shape factor cannot bridge the gap between experimental curve and extrapolated straight line. Convex curvature downwards of the population density plot may be produced when the crystal growth rate decreases with increasing crystal size. In the present case, the system is likely to have such a size dependency in the large-size range.

Because of abrasion due to crystal-crystallizer or crystal-crystal collisions the net growth rate of a crystal may diminish, so that a crystal will grow into a subsequent fraction at a reduced rate. Since a constant percentage of crystals of each fraction is constantly being removed, this must result in a steadily greater reduction in the population density with increasing crystal size. The net growth rate may even become zero when the abrasion rate equals the rate of mass transfer to the crystal. In that case the population density approaches zero. From the experimental curves it is found that the extent of curvature increased with impeller speed, the period of time that the crystals are exposed to the abrasive conditions and the magma concentration. The effect of impeller speed is however of greatest importance. The effect of impeller speed on the extent of curvature is best illustrated by Figure 8.

The observed influence of magma concentration on the shape of the CSD in the largest size range indicates that crystal-crystal collisions play a role. The possible contribution of this type of collisions to the overall nucleation rate is however small, since the number of large crystals is relatively small. Further, it has been found that the degree of curvature exhibited by the CSD is usually larger for the pitched blade impeller. This may indicate that the abrasion rate is a function of impact probability and energy, which are without any doubt greater for the pitched blade impeller than for the marine propeller. The effect is demonstrated in Figure 4.

Further the shape of the CSD in the large size range suggests, that the abrasion rate increases with increasing crystal size. This could be explained on basis of the increasing impact energy and, as will be demonstrated later, impact frequency with increasing size.

Finally comparison of the CSD's obtained in the 55 litre and 91 litre crystallizer indicates that for identical speed, residence time and magma concentration the CSD from the 91-L crystallizer systematically exhibits less curvature. Also less rounding of crystals is observed. This scale-effect is illustrated in Figure 9.

These observations suggest, that the crystals in the 91-L crystallizer exhibit a lower abrasion rate. This can be attributed to the reduced collision frequency per crystal due to the longer turnover time in the 91-L crystallizer. It will be obvious, that the state of rounding of a crystal is dominated by the number of impacts ex-

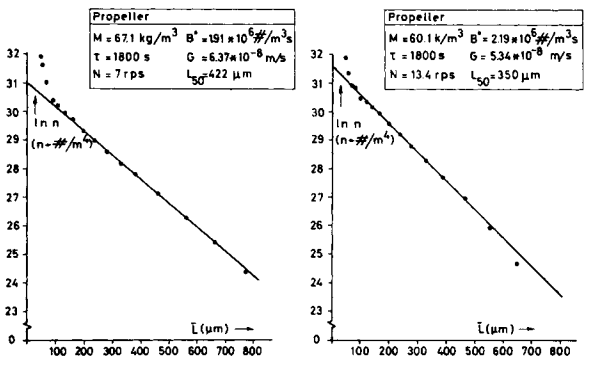

Figure 8. Effect of impeller speed on the degree of curvature.

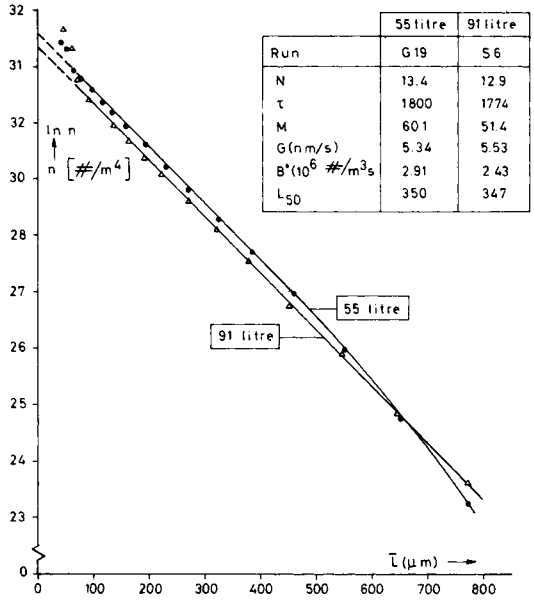

Run	55 litre G19	91 litre S6
N	13.4	12.9
τ	1800	1774
M	60.1	51.4
G(nm/s)	5.34	5.53
$B^o(10^6$ #/m³s	2.91	2.43
L_{50}	350	347

Figure 9. Effect of crystallizer scale: marine propeller.

erted on that particular crystal as well as the impact energy. Both will be a function of impeller speed and design as well as the size and the circulation frequency of the colliding crystal.

It needs no argument, that, contrary to the secondary nucleation process, the turnover time certainly has significance in the scale-up of the abrasion process.

COLLISION FREQUENCIES

In order to get more insight in the relation between collision frequency, crystal size and impeller speed, experiments have been carried out, which have been designed to determine *in situ* impact forces between particle and impeller blade. The method, which was initially developed by Bemer (1979), also enabled the evaluation of collision frequencies.

Equipment

In order to measure collision frequencies between particles and impeller a measuring device has been built into one of the blades of a six-bladed disc turbine. Requiring high sensitivity and a high response frequency, piezo ceramic elements were found to be suitable as a force transducer. Two piezo ceramic discs (Philips type PXE-5, sensitivity 12.10^{-6} V.m²/N; resp. freq. 0,1 μs) were built in. Signals were first amplified, transmitted through slip-contacts and recorded on an oscilloscope. A schematic diagram of the impact meter is given in Figure 10.

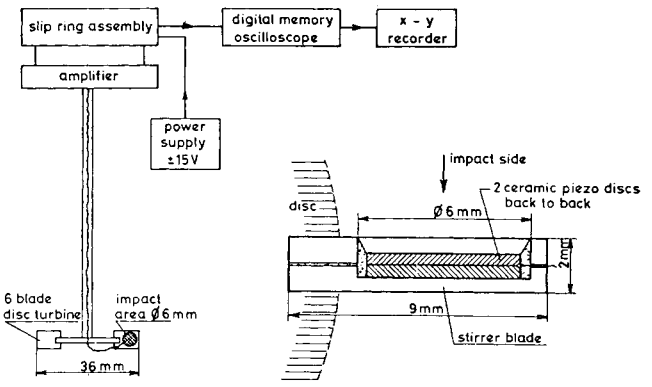

Figure 10. Impact meter.

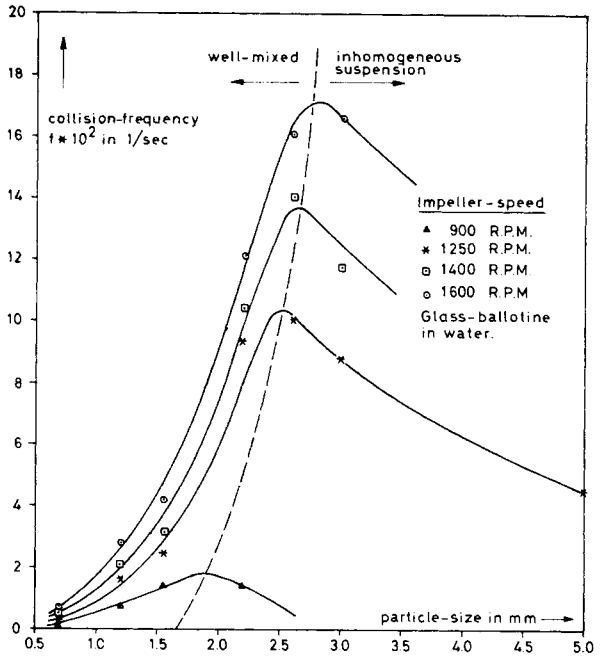

Figure 11. Particle-impeller collision-frequencies on back of impeller-blade

Results and Discussion

The impact meter as described above has been used in a flat bottom 1-L vessel to determine collision frequencies for glass ballitini in water. Preliminary results have been shown in Figure 11. In this figure the collision frequency per particle per blade has been plotted versus particle-size for various impeller speeds.

Although impeller-design and vessel geometry deviate from the crystallizer geometry the results at least qualitatively suggests that collision frequencies strongly increase with increasing crystal size. A small crystal may be able to follow better the flow round the impeller. The decrease in frequency at very large particle sizes can be attributed to non homogeneous suspension. Further the effect of impeller speed on collision frequencies is very pronounced. For constant particle size an almost linear increase in collision frequency with increasing impeller speed is found.

Although the results presented only have qualitative value, they may contribute to the knowledge of the relation between frequency and energy of crystal collisions and the hydrodynamics of the crystallizer. Such knowledge may lead to a better understanding of the interaction of process configuration and operating conditions with system kinetics.

ACKNOWLEDGMENT

The authors acknowledge the financial support provided by Imperial Chemical Industries Ltd., Mond Division, Technical Department.

NOTATION

B^o = nucleation rate, #/m³s
ΔC = supersaturation, kg/m³
d = impeller-diameter, m
G = crystal growth rate, m/s nm/s
h, i, j = nucleation parameters
k = nucleation constant
k_B = nucleation constant
k_p = pump constant
k_v = volume shape factor
L = crystal size, m/μm
L_{50} = mean crystal size, m/μm

M = magma concentration, kg/m^3
n = population density, #/m^4
n^o = nuclei population density, #/m^4
N = impeller speed, s^{-1}
p = exponent
P = power input, W
P_o = power number
s = exponent
ϵ = specific power input, W/kg
μ = moment of crystal size distribution
ρ = density, kg/m^3
ρ_s = solids density, kg/m^3
τ = residence time, s
ϕ_{mv} = vapor load, kg/s
ϕ_v = volumetric flow rate, m^3/s

LITERATURE CITED

Asselbergs, C. J. and E. J. De Jong, "Some theoretical aspects of the population density distribution in a NaCl evaporating crystallizer with external circulation," Proc. 5th Symp. on Industrial Crystallization, CHISA (1972).

Bemer, G. G., "Agglomeration in suspension: A study of mechanisms and kinetics," Ph.D. Thesis, Delft University of Technology (1979).

Bujac, P. D. B., "Attrition and secondary nucleation in agitated crystal slurries," *Indus. Crystallization*, **23**, J. W. Mullin, ed. Plenum Press, New York (1976).

Evans, T. W., G. Margolis, and A. F. Sarofim, "Mechanisms of secondary nucleation in agitated crystallizers," *AIChE J.*, **20**, 950 (1974).

Garabedian, H., and R. F. Strickland-Constable, "Collision breeding of crystal nuclei: sodium chlorate," *J. Cryst. Growth.*, **13**, 506 (1972).

Grootscholten, P. A. M., C. J. Asselbergs, and E. J. De Jong, "Relevance of pilot scale research," 73rd AIChE Annual Meeting, Chicago (1980).

Johnson R. T., R. W. Rousseau, and W. L. McCabe, "Factors affecting contact nucleation," *AIChE Symp. Ser.*, **68**, 31 (1972).

Koros, W. J., D. A. Dalrymple, R. P. Kuhlman, and N. F. Brockmeier, "Crystallization of sodium chloride in a continuous mixed-suspension crystallizer," *AIChE Symp. Ser.*, **68**, 67 (1972).

Van't Land, C. M., and B. G. Wienk, "Control of particle size in industrial NaCl-crystallization," *Indus. Crystallization*, **51**, J. W. Mullin ed., Plenum Press, New York (1976).

Larson, M. A., and L. L. Bendig, "Nuclei generation from repetitive contacting," *AIChE Symp. Ser.*, **72**, 21 (1976).

Liu, Yih-An, and G. D. Botsaris, "Impurity effects in continuous-flow mixed suspension crystallizers," *AIChE J.*, **19**, 510 (1973).

Randolph, A. D., and S. K. Sikdar, "Effect of soft impeller coating on the net formation of secondary nuclei," *AIChE J.*, **20**, 410 (1974).

Rousseau, R. W., K. K. Li, and W. L. McCabe, "The influence of seed crystal size on nucleation rates," *AIChE Symp. Ser.*, **72**, 48 (1976).

Scrutton, A., "Laboratory study of the crystallization of sodium chloride from brine," 5th Symposium on Salt, Hamburg (1979).

Scrutton, A., and P. A. M. Grootscholten, "A Study on the dissolution and growth of sodium chloride crystals, *Trans. Inst. Chem. Engrs.* (Oct., 1981).

Shah, B. C., W. L. McCabe, and R. W. Rousseau, "Polyethylene vs stainless steel impellers for crystallization processes," *AIChE J.*, **19**, 194 (1973).

Tai, C. Y., W. L. McCabe, and R. W. Rousseau, "Contact nucleation of various crystal types," *AIChE J.*, **21**, 351 (1975).

Youngquist, G. R., J. Estrin, R. Jaganathan, and C. Y. Sung, "Secondary nucleation by fluid shear," 67th AIChE Annual Meeting, Washington (1974).

Manuscript received May 13, 1981; revision received October 13, and accepted October 28, 1981.

Kinetics of Thermal Regeneration Reaction of Activated Carbons used in Waste Water Treatment

The kinetics of the thermal regeneration of activated carbons used in the waste water treatment was analyzed on the basis of a model that the regeneration reaction consists of a set of many first-order reactions each of which has different activation energy and frequency factor. The frequency factors were correlated approximately by a function of the activation energy.

The difference in the activation energy was represented by a distribution curve which was obtained by analyzing the thermogravimetric curve (TG curve) measured under a constant heating rate. The weight loss during the regeneration reaction under complicated heating conditions was well predicted by use of the distribution curve determined by the proposed method. This method describing the kinetics of the thermal regeneration may be applied to the design of reactors regenerating spent carbons.

KENJI HASHIMOTO,
KOUICHI MIURA
and
TSUNEO WATANABE

Department of Chemical Engineering
Kyoto University
Kyoto, Japan

SCOPE

Activated carbons have been widely used in adsorption processes for the purpose of the removal of toxic substances, the recovery of valuable substances, the fractionation of mixtures, and so on. In recent years, advanced waste water treatment using activated carbons has received much attention. Since activated carbons are rather expensive, the spent carbons are used again and again by repeating the regeneration. Several methods such as thermal regeneration, chemical regeneration, biological regeneration, and solvent extraction have been proposed for the regeneration of spent carbons (Loven, 1973). Of these methods, thermal regeneration is by far the one most commonly used. Thermal regeneration is usually performed in